RSC Advances

PAPER

View Article Online
View Journal | View Issue

Cite this: *RSC Adv.*, 2014, **4**, 34987

Optical phonon behaviors and unstable polar mode in transparent conducting $Ba_{1-x}La_xSnO_3$ films from temperature dependent far-infrared reflectance spectra

Chao Shan, Ping Chang, Kai Shi, Yawei Li, Zhigao Hu* and Junhao Chu

Received 5th May 2014
Accepted 24th July 2014

DOI: 10.1039/c4ra04100c

www.rsc.org/advances

We report lattice vibration behaviors of transparent conducting $Ba_{1-x}La_xSnO_3$ films derived from the far-infrared reflectance spectra in the temperature range of 105–300 K. Three main phonon modes can be observed at room temperature and the frequencies approximately decrease with increasing La content. A polar mode TO_1 appears at about 137 cm^{-1} and becomes unstable with decreasing temperature. On cooling, the TO_1 mode vanishes at 270, 240, 180 and 210 K for the films with $x = 0.00$, 0.02, 0.04 and 0.06 and appears again with further decreasing of the temperature for the La content of 0.00 and 0.02. It can be explained by the reversal of the TO_1 mode effective charge, which originates from a drastic change of the $O_{2/3}$ eigendisplacement. The content dependent phonon behaviors are mainly caused by octahedral tilting with substituting La for Ba.

1 Introduction

Perovskite-structured oxide is an important class of materials, possessing many diverse physical properties including optical transparency, ferroelectricity, piezoelectricity, superconductivity, and photocatalytic activity.[1,2] Furthermore, the epitaxial all-perovskite multilayer heterostructures have attracted much attention due to the multiplicity of physical properties of perovskites and advantages in film growth. These all-perovskite multilayer heterostructures are promising candidates for innovative micro- and nanoelectronic devices.[3,4] Alkaline earth stannates with the general formula $ASnO_3$ (A = Ba, Sr, and Ca) are another perovskite system, which are frequently used in the electronic industry owing to the interesting dielectric and gas-sensing properties.[5,6] Perovskite stannates exhibit different structures at room temperature: $CaSnO_3$ and $SrSnO_3$ are orthorhombic (space group *Pnma*). $BaSnO_3$ (BSO), on the contrary, is perfectly cubic at room temperature and zero pressure (space group $Pm\bar{3}m$). It was confirmed by a number of experiments and suggested by its Goldschmidt tolerance factor $t = 1.02$, which is higher than those of other stannates.[7] BSO behaves as an n-type semiconductor with a wide band gap (about 4 eV) and remains stable at temperatures up to 1000 °C.[8] Therefore, it can be used in thermally stable capacitors, humidity sensors and gas sensors.[9,10]

Recently, a transparent BSO system has been reported to possess electron mobilities when doped with La.[11–14] Kim *et al.* reported single-crystal $Ba_{1-x}La_xSnO_3$ (BLSO) with a mobility of 320 $cm^2 V^{-1} s^{-1}$ for a carrier concentration of 8×10^{19} cm^{-3}.[12] It is the highest value reported for any transparent conducting oxide, which can be applied in optoelectronic devices. The high mobility is derived from the small electron effective mass due to the antibonding *s* character at the conduction band minimum state.[15] Moreover, two interband absorptions were observed from the dielectric function and the peak transition energy increased linearly with increasing La content.[16] In those studies, much effort had been focused on the electrical transport properties and band structure by optical measurements from the ultraviolet to near-infrared region. However, the far-infrared (FIR) optical properties of the BLSO films are still insufficient. Generally, the FIR reflectance technique can be used to estimate infrared (IR)-active phonons of semiconductor materials, which is based on the potentially different selection rules and the penetration of the exciting radiation. Lattice vibrations and IR dielectric functions of BLSO films not only provide basic optical properties but will also be critical for developing the novel materials for optoelectronic applications. Moreover, they are helpful for estimating carrier concentration and electrical transport properties.

In BSO, the Sn ion forms an octahedron with oxygen, and the SnO_6 octahedra are linked in three dimensional networks with corners sharing oxygen.[17] Kim *et al.* calculated the phonon spectra of BSO in the Heyd, Scuseria, and Ernzerhof (HSE06) hybrid functional level. They confirmed that BSO has three IR active modes (TO_1, TO_2, and TO_3) without Raman active

Key Laboratory of Polar Materials and Devices, Ministry of Education, Department of Electronic Engineering, East China Normal University, Shanghai 200241, China. E-mail: zghu@ee.ecnu.edu.cn; Fax: +86-21-54345119; Tel: +86-21-54345150

modes.[18] Although there are some reports about the vibrational properties of BSO using theoretical calculations, a systematic experimental study has not yet been carried out, especially for La doped BSO. In the article, $Ba_{1-x}La_xSnO_3$ (x = 0–0.06) films were prepared by the sol–gel route and the effects of La substitution on the phonon modes have been investigated by FIR reflectance spectra at low temperature. It was found that the octahedral tilting caused by La substitution strongly affects the behaviors of lattice vibration.

2 Experimental section

The BLSO (x = 0, 0.02, 0.04 and 0.06, hereafter denoted as BSO, BLSO0.02, BLSO0.04 and BLSO0.06, respectively.) films were directly deposited on (0001) sapphire substrates by a sol–gel method.[16] The temperature dependent infrared reflectance spectra of the BLSO films were recorded by a Bruker VERTEX 80V Fourier transform infrared (FTIR) spectrometer with a specular reflectance setup. The incident angle was set to about 6° and the spectral resolution was selected as 2 cm^{-1}. The FIR spectra were measured in the frequency range of 100–700 cm^{-1} by a globar lamp (an U-shaped SiC piece), a 6 μm Mylar beamsplitter, and a pyroelectric DLaTGS detector. The sapphire and BLSO films were mounted into an Oxford AC-V12w continuous flow cryostat with the samples in He vapor. The temperature could be varied from 105 to 300 K within the accuracy of 0.1 K. The cryostat was equipped with polypropylene windows for the FIR region. Note that a gold mirror whose absolute reflectance was measured was taken as a reference for the spectra at the corresponding temperatures.

3 Results and discussion

To extract the dielectric functions and other physical parameters of the BLSO films, the IR reflectance spectra were analyzed by a multilayer model with a three-phase structure (air/BLSO/substrate). The IR dielectric response functions can be typically expressed by the Lorentz multi-oscillator model for the optical phonons, which can be written as:

$$\varepsilon(E) = \varepsilon_\infty + \sum_{n=1}^{3} \frac{A_n {E_n}^2}{{E_n}^2 - E^2 - i\mathrm{Br}_n E}. \quad (1)$$

where E is the frequency of the incident light, E_n is the phonon frequency, A_n is the oscillator strength, Br_n stands for the phonon broadening, and ε_∞ represents the dielectric constant at frequencies above the measured optical phonons. In addition, a Drude term $\varepsilon(E) = -\frac{D_p C}{E^2 + iCE}$ was added for BLSO (x = 0.02, 0.04, and 0.06) films to account for free carrier contribution.[19] The formula depends on the following two parameters: the oscillator strength D_p, and the broadening term C. The experimental reflectance spectra of the sapphire substrate at different temperatures have been fitted using the Lorentz model without the Drude term. The phonon modes near 385, 440, 569, and 633 cm^{-1} belong to the vibrations from the sapphire substrate.[20,21] These fitting parameters were used for reproducing the reflectance spectra of the $Ba_{1-x}La_xSnO_3$ films with the La composition from 0.00 to 0.06 at various temperatures. Note that the thicknesses of the BLSO films measured by cross-sectional scanning electron microscopy are 272, 254, 266 and 257 nm for x = 0.00, 0.02, 0.04 and 0.06, respectively.[16] The best-fit parameter values of the Lorentz and Drude model with errors are summarized in Table 1. The reproduced IR reflectance spectra are also plotted as solid lines in Fig. 1, indicating a good agreement within the experimental errors.

The dielectric functions of the BLSO films at room temperature derived from fitting FIR reflectance spectra are shown in Fig. 2(a). Three main lattice vibration modes are observed from the dielectric functions, which are similar to those derived by FIR ellipsometry at room temperature,[19] and in accordance with group theory predictions. For the cubic perovskite, the normal modes of the lattice vibration at the zone center are given in the irreducible representation (irrep.) by: $\Gamma = 4T_{1u} + T_{2u}$. One of the T_{1u} modes corresponds to the acoustic phonon mode, while the T_{2u} mode is optically silent, *i.e.*, neither IR nor Raman active.[22] The remaining three T_{1u} modes are IR active, corresponding to the following vibrational motions: Sn–O bond distance modulation (stretching mode), translational motion of barium atoms with respect to the SnO_3 lattice (external mode) and Sn–O–Sn bond angle modulation (bending mode).[22] In BSO, the heavier Ba atom contributes mainly to the lower frequency mode, whereas the Sn atom contributes to the intermediate frequency mode. The O atom contribution to the higher frequency mode is dominant because its atomic mass is much lighter than those of the other atoms.[18] As shown in Fig. 2(b), the TO_1 mode occurs at about 137 cm^{-1}, which is assigned to the movement of Ba ions up and down (and SnO_6 tetrahedra up and down). The TO_2 mode appears at 253 cm^{-1}, corresponding to a Sn–O–Sn scissor movement. The TO_3 vibration can be seen at about 614 cm^{-1}, which is related to the symmetrical Sn–O–Sn stretching. Due to the macroscopic vertical polarization field of BLSO films, the frequency of the LO mode is larger than that of the corresponding TO mode, *i.e.*, so-called TO–LO splitting. While the TO phonons appear as sharp peaks in the ε_2 spectra, the corresponding LO frequencies can be determined from the maxima of the loss function $-\mathrm{Im}[\varepsilon^{-1}(E)]$ that are close to the zero of the ε_1 spectra [Fig. 2(a)]. The frequencies of LO_1 and LO_2 for BSO are about 150 and 432 cm^{-1}. However, the frequency of LO_3 is beyond our measurement range.

Fig. 2(b) shows the phonon frequencies of TO_1, TO_2 and TO_3 with different La content. As can be seen, the frequencies of the TO_1 and TO_2 modes decrease with an increase in La content from 0.00 to 0.04. However, the phonon modes shift towards a higher frequency for the BLSO0.06 film. For TO_3, unlike TO_1 and TO_2, the frequency keeps decreasing with increasing La content beyond 0.04. For studying the stability and geometric distortion of a perovskite ABO_3 structure, the Goldschmidt tolerance factor is very helpful. For $BaSnO_3$, it is defined by $t = (r_{Ba} + r_O)/\sqrt{2}(r_{Sn} + r_O)$. Here, the Shannon's values of the ionic radius (r_{Ba} = 1.61 Å, r_{La} = 1.36 Å, r_{Sn} = 0.69 Å, r_O = 1.40 Å) are used.[23] It can be seen that the Goldschmidt tolerance factor decreases with substituting La (1.36 Å) for Ba (1.61 Å), indicating octahedral tilting; *i.e.*, the crystal symmetry on the

Table 1 Parameter values of the Lorentz and Drude dielectric function model for the $Ba_{1-x}La_xSnO_3$ films determined from the simulation of the IR reflectance spectra in Fig. 1. The 90% reliability is given in parentheses

Samples			TO_1 (cm^{-1})			TO_2 (cm^{-1})			TO_3 (cm^{-1})			Drude (cm^{-1})	
x		ε_∞	A_1	E_1	Br_1	A_2	E_2	Br_2	A_3	E_3	Br_3	D_p ($\times 10^3$)	C ($\times 10^2$)
0.00	300 K	1.2 (0.3)	1.1 (0.2)	138 (1)	7 (2.6)	4.7 (0.1)	254 (0.4)	16.6 (0.8)	1.1 (0.1)	623 (0.7)	66.8 (2.3)	—	—
	105 K	3 (0.4)	2.4 (0.2)	135 (0.4)	10.4 (1)	9.3 (0.4)	255 (1.2)	36.7 (2.7)	0.8 (0.1)	627 (0.5)	36.1 (0.4)	—	—
0.02	285 K	1.2 (0.4)	0.5 (0.2)	138 (0.9)	3.8 (2.6)	5.7 (0.2)	254 (0.4)	17.4 (0.9)	0.8 (0.1)	620 (0.7)	42.6 (2.6)	1.3 (0.4)	12.2 (3.7)
	225 K	0.9 (0.4)	—	—	—	5.8 (0.2)	253 (0.4)	14.8 (0.9)	0.9 (0.1)	623 (0.7)	41.4 (2.2)	2.5 (0.1)	4.8 (0.6)
0.04	270 K	3 (1)	0.4 (0.5)	137 (1.8)	2.9 (0.9)	7.1 (0.5)	253 (0.9)	21.7 (2.3)	0.5 (0.1)	616 (1.2)	28 (4.8)	7.2 (1.3)	11.9 (2.2)
	135 K	3.4 (1.3)	—	—	—	5 (0.9)	252 (1.3)	9.6 (3.1)	0.6 (0.2)	621 (2)	24.3 (6.9)	10 (0.1)	7.3 (1.6)
0.06	255 K	3.2 (0.9)	0.9 (0.5)	136 (2.6)	6.4 (7.8)	8.1 (0.7)	254 (1.3)	36.3 (3.8)	0.8 (0.1)	626 (1.6)	48.8 (6.5)	5.1 (1.2)	10.9 (3.1)
	180 K	5.3 (1.4)	—	—	—	4.6 (0.7)	251 (1.3)	14.5 (3.2)	0.8 (0.2)	627 (2.1)	43.6 (7.1)	6.9 (0.5)	6.7 (1.3)

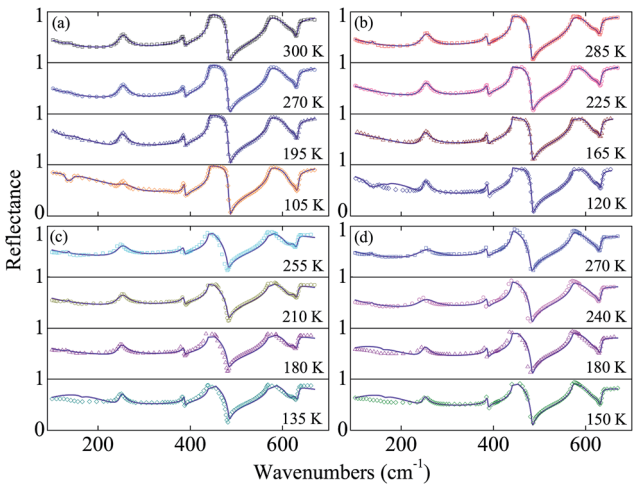

Fig. 1 Experimental far-IR reflectance spectra (dotted lines) and best-fit results (solid lines) for the BLSO films [(a) $x = 0$, (b) $x = 0.02$, (c) $x = 0.04$ and (d) $x = 0.06$] at different temperatures.

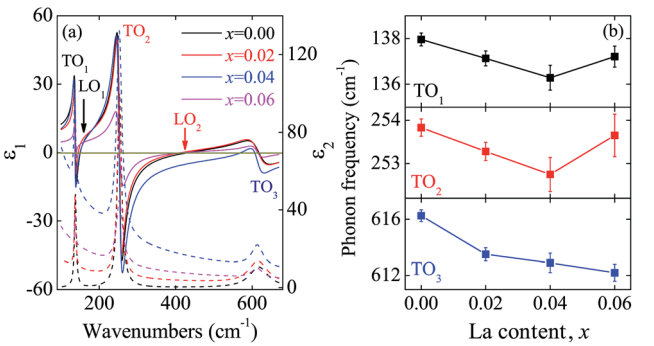

Fig. 2 (a) The real part (ε_1, solid lines) and imaginary part (ε_2, dashed lines) of the dielectric functions for the BLSO films at room temperature. (b) The phonon frequency variation of TO_1, TO_2 and TO_3 modes with different La content at room temperature.

microscopic level lowers from cubic to orthorhombic.[24] The X-ray diffraction (XRD) results from our previous work show that the positions (2θ) of the stronger (110) diffraction peaks are located at about 30.92, 30.97, 31.15, and 31.06°.[16] The (110) diffraction peaks shift towards the high-angle direction, indicating increased octahedral tilting. It is worth noting that the phonons TO_1 and TO_2 have the same variation tendency as the (110) diffractions with increasing La content. Therefore, it can be concluded that the shifts of phonon frequencies with different La content can originate from the octahedral tilting.

To further understand the intrinsic characteristics of the BLSO films, the temperature dependence of the far-IR reflectance spectra is shown in Fig. 1. At high temperatures all three phonon modes can be observed. On cooling, the phonon frequencies and strengths change regularly. The TO_1 modes present a shift to a lower frequency at first and then shift to a higher frequency for the BSO and BLSO0.02 films. The TO_2 modes from the four films present a shift to a lower frequency and the phonon broadening decreases with decreasing temperature from 300 to 105 K (Table 1). However, the TO_3 modes shift towards a higher frequency with decreasing the temperature. The behaviors for TO_1, TO_2 and TO_3 can be simply ascribed to thermal expansion of lattice. An interesting feature is that TO_1 vanishes at some typical temperatures, such as the spectra at 240 K for the BSO film and at 180 K for the BLSO0.06 film. However, on further decreasing the temperature, the TO_1 mode appears again for the BSO and BLSO0.02 films. For instance, there is a deep trough in the spectrum at 105 K for the BSO film. For the films with $x = 0.04$ and 0.06, unlike the other two samples, the TO_1 mode does not appear again. To our knowledge, in titanate, zirconate, and niobate perovskites, the TO_1 mode does not vanish with decreasing temperature. Thus, the phenomenon of the temperature dependent TO_1 mode of

BLSO could be specific to stannates. The temperature dependence of the dielectric functions for the BLSO films is shown in Fig. 3. The dielectric functions of all four films change sharply in the frequency region of 100–200 cm^{-1}, especially for the BSO and BLSO0.02 films. In addition, ε_2 increases with decreasing frequency for the BLSO0.02, BLSO0.04 and BLSO0.06 films, which could be explained by the shift of the plasma frequency ω_p with carrier concentration n [$n = \frac{\varepsilon_0 m^* D_p C}{\hbar^2 e^2}$,[16] where ε_0 is the permittivity of free space, m^* is the effective mass, e is the electronic charge, $\hbar$ is $h/2\pi$ (h is Plank's constant), and D_p and C are the parameters of the Drude model (Table 1)]. The results indicate that there is an unstable polar mode (TO_1) in the present BLSO system.

To demonstrate the unstable mode clearly, the temperature dependent TO_1 phonon frequency is plotted in Fig. 4(a). As can be seen, the TO_1 mode vanishes in the temperature range from 270 to 195 K, 240 to 150 K, 180 to 105 K and 210 to 105 K for the BSO, BLSO0.02, BLSO0.04 and BLSO0.06 films, respectively. Structural phase transitions in ABO_3 oxide perovskites are of intrinsic interest as well as being tied to more complex phenomena such as photon–lattice couplings. Anyway, other perovskite stannates with smaller cations on the A site, and thus lower tolerance factors, such as $SrSnO_3$ and $CaSnO_3$, exhibit structural distortions. $SrSnO_3$ even presents a complex succession of phase transitions with temperature.[25] However, the $BaSnO_3$ compound does not present any transition to a lower symmetry structure even at 10 K, keeping its high symmetry cubic structure, as suggested by theoretical calculations and XRD experiments.[26] According to group theory ($Pm\bar{3}m$), the TO_1 mode does exist even at temperatures as low as 10 K. The reason for TO_1 vanishing in the present IR reflectance spectra is that the mode becomes IR inactive. As we know, an IR photon can only couple with the polar optic transverse phonon mode at the center of the Brillouin zone. Thus, the TO_1 mode becomes nonpolar from polar with decreasing temperature, *i.e.*, the TO_1 mode can not couple with an electric field at some temperatures.

Since the mode effective charge (MEC) indicates how strongly a phonon mode couples with an electric field, we now focus on the MEC, defined for each TO mode (τ) as the following:

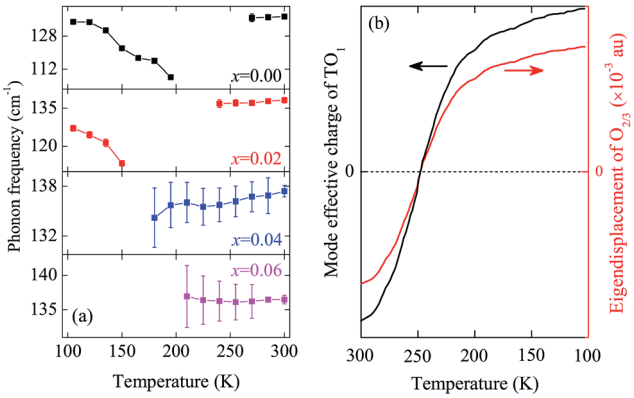

Fig. 4 (a) Temperature dependence of the TO_1 mode for the BLSO films. (b) The schematic mode effective charge and eigendisplacement of the TO_1 mode with the temperature region of 105–300 K.

$$Z_\alpha^{*(\tau)} = \sum_{i,\beta} \frac{Z_{\alpha\beta}^{*(i)} e_{i\beta}^{(\tau)}}{||e^{(\tau)}||}. \quad (2)$$

here $Z_{\alpha\beta}^{*(i)}$ is the Born effective charge tensor of atom (i) (i runs over all the atoms of the cubic unit cell) and e^τ is the phonon eigendisplacement vector associated with the mode (τ). The Born effective charge $Z_{\alpha\beta}^{*(i)}$ is the first derivative of the macroscopic polarization P_α (along the α direction) with respect to the displacement of atom (i) along the β direction. Since the Born effective charge evolves slowly with temperature,[27] the mode effective charge is proportional to the polarization induced by atomic motions that follow the eigendisplacement vector e^τ. As we know, the lattice parameter decreases with decreasing temperature. It can result in a strong modification of the eigendisplacements of $O_{2/3}$, while the eigendisplacements of Ba, Sn, and O_1 change slowly.[28] As shown in Fig. 4(b), the MEC of TO_1 is mainly affected by the eigendisplacements of $O_{2/3}$. Both the normalized eigendisplacement of $O_{2/3}$ and the MEC of TO_1 changes from negative to positive with decreasing temperature and vanishes at a specific temperature (T_s). This suggests a drastic lowering in the dielectric response of BLSO at such temperature, since only TO_2 and TO_3 contribute to the dielectric constant (Fig. 3), and explains well the present data derived from the FIR reflectance spectra. With decreasing the

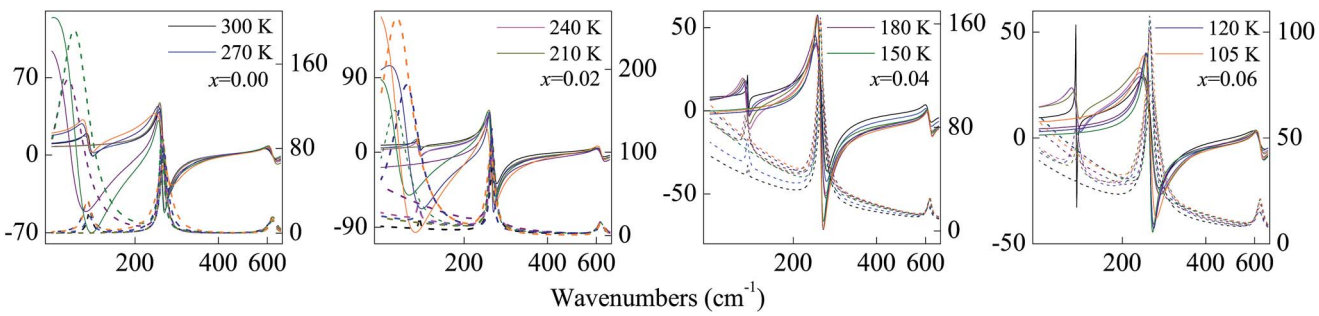

Fig. 3 The real part (ε_1, solid lines) and imaginary part (ε_2, dashed lines) of the dielectric functions for the BLSO films at different temperatures. In each graph, the real and imaginary parts can be referred to the left and right axis, respectively. Note that the logarithmic coordinate is applied for the horizontal x-axis.

temperature from 300 K, the value of MEC decreases, corresponding to the intensities of the TO_1 modes degenerating at high temperature. When the temperature (lattice parameter) decreases to a specific value (or region), the MEC of TO_1 is zero (or close to zero), resulting in the absence of TO_1. On further cooling, the MEC reverses to the opposite sign, corresponding to the deep trough at about 130 cm^{-1} in the low temperature reflectance spectra. Furthermore, the T_s for MEC decreasing to zero is 270, 240, 180, and 210 K for the films with $x = 0.00$, 0.02, 0.04, and 0.06, respectively. Note that the T_s also has the same variation tendency as the (110) diffractions with increasing La content. From the present results, we can conclude that the MEC becomes insensitive to temperature with the increasing octahedral tilting at 300 K.

4 Conclusion

In conclusion, the La content dependence of the phonon modes in $Ba_{1-x}La_xSnO_3$ (x = 0–0.06) films have been investigated by FIR reflectance spectra in the temperature range of 105–300 K. Three phonon modes can be seen in the frequency range of 100–700 cm^{-1}. An interesting unstable polar mode TO_1 has been observed at low temperature for the BLSO films. We have explained the phenomena by the increase of the TO_1 mode effective charge, which originates from a drastic change of the $O_{2/3}$ eigendisplacement.

Acknowledgements

This work was financially supported by the Major State Basic Research Development Program of China (Grant nos. 2011CB922200 and 2013CB922300), Natural Science Foundation of China (Grant nos. 11374097, and 61376129), Projects of Science and Technology Commission of Shanghai Municipality (Grant nos. 14XD1401500, 13JC1402100, and 13JC1404200), and the Program for Professor of Special Appointment (Eastern Scholar) at Shanghai Institutions of Higher Learning.

Notes and references

1 T. Wolfram and S. Elliatioglu, *Electronic and Optical Properties of d-Band Perovskites*, Cambridge University Press, New York, 2006.
2 P. Mandal, S. S. Bhat, Y. Sundarayya, A. Sundaresan, C. N. R. Rao, V. Caignaert, B. Raveau and E. Suard, *RSC Adv.*, 2012, **2**, 292–297.
3 J. Son, P. Moetakef, B. Jalan, O. Bierwagen, N. J. Wright, R. Engel-Herbert and S. Stemmer, *Nat. Mater.*, 2010, **9**, 482.
4 A. Ohtomo and H. Y. Hwang, *Nature*, 2004, **427**, 423–426.
5 L. Geske, V. Lorenz, T. Muller, L. Jager, H. Beige, H. P. Abicht and V. Mueller, *J. Eur. Ceram. Soc.*, 2005, **25**, 2537–2542.
6 S. W. Tao, F. Gao, X. Q. Liu and O. T. Srensen, *Sens. Actuators, B*, 2000, **71**, 223–227.
7 T. Maekawa, K. Kurosaki and S. Yamanaka, *J. Alloys Compd.*, 2006, **416**, 214–217.
8 B. Ostrick, M. Fleischer and H. Meixner, *J. Am. Ceram. Soc.*, 1997, **80**, 2153–2156.
9 U. Lampe, J. Gerblinger and H. Meixner, *Sens. Actuators, B*, 1995, **26**, 97–98.
10 S. V. Manorama, C. V. G. Reddy and V. J. Rao, *Appl. Surf. Sci.*, 2001, **174**, 93–105.
11 X. Luo, Y. S. Oh, A. Sirenko, P. Gao, T. A. Tyson, K. Char and S. W. Cheong, *Appl. Phys. Lett.*, 2012, **100**, 172112.
12 H. J. Kim, U. Kim, H. M. Kim, T. H. Kim, H. S. Mun, B. G. Jeon, K. T. Hong, W. J. Lee, C. Ju, K. H. Kim and K. Char, *Appl. Phys. Express*, 2012, **5**, 061102.
13 Q. Z. Liu, J. J. Liu, B. Li, H. Li, G. P. Zhu, K. Dai, Z. L. Liu, P. Zhang and J. M. Dai, *Appl. Phys. Lett.*, 2012, **101**, 241901.
14 S. Sallis, D. O. Scanlon, S. C. Chae, N. F. Quackenbush, D. A. Fischer, J. C. Woicik, J.-H. Guo, S. W. Cheong and L. F. J. Piper, *Appl. Phys. Lett.*, 2013, **103**, 042105.
15 H. R. Liu, J. H. Yang, H. J. Xiang, X. G. Gong and S. H. Wei, *Appl. Phys. Lett.*, 2013, **102**, 112109.
16 C. Shan, T. Huang, J. Z. Zhang, M. J. Han, Y. W. Li, Z. G. Hu and J. H. Chu, *J. Phys. Chem. C*, 2014, **118**, 6994–7001.
17 D. J. Singh, D. A. Papaconstantopoulos, J. P. Julien and F. Cyrot-Lackmann, *Phys. Rev. B: Condens. Matter Mater. Phys.*, 1991, **44**, 9519–9523.
18 B. G. Kim, J. Y. Jo and S. W. Cheong, *J. Solid State Chem.*, 2013, **197**, 134–138.
19 T. N. Stanislavchuk, A. A. Sirenko, A. P. Litvinchuk, X. Luo and S. W. Cheong, *J. Appl. Phys.*, 2012, **112**, 044108.
20 Z. G. Hu, M. Strassburg, N. Dietz, A. G. U. Perera, A. Asghar and I. T. Ferguson, *Phys. Rev. B: Condens. Matter Mater. Phys.*, 2005, **72**, 245326.
21 X. R. Li, M. J. Han, P. Chang, Z. G. Hu, Y. W. Li, Z. Q. Zhu and J. H. Chu, *Appl. Phys. Lett.*, 2014, **104**, 012103.
22 M. Licheron, G. Jouan and E. Husson, *J. Eur. Ceram. Soc.*, 1997, **17**, 1453–1457.
23 R. D. Shannon, *Acta Crystallogr.*, 1976, **32**, 751–767.
24 W. F. Zhang, J. W. Tang and J. H. Ye, *J. Mater. Res.*, 2007, **22**, 1859–1871.
25 E. H. Mountstevens and S. A. T. Redfern, *Phys. Rev. B: Condens. Matter Mater. Phys.*, 2005, **71**, 220102.
26 É. Bévillon, A. Chesnaud, Y. Z. Wang, G. Dezanneau and G. Geneste, *J. Phys.: Condens. Matter*, 2008, **20**, 145217.
27 Ph. Ghosez, X. Gonze, Ph. Lambin and J. P. Michenaud, *Phys. Rev. B: Condens. Matter Mater. Phys.*, 1995, **51**, 6765.
28 É. Bévillon and G. Geneste, *Phys. Rev. B: Condens. Matter Mater. Phys.*, 2007, **75**, 214106.